Variations in Microanatomy of the Human Modiolus: Implications for Cochlear Implants

Markus Pietsch (markus.pietsch@helios-gesundheit.de)
Hannover Medical School
Daniel Schurzig
Hannover Medical School
Rolf Salcher
Hannover Medical School
Athanasia Warnecke
Hannover Medical School
Peter Erfurt
Hannover Medical School
Thomas Lenarz
Hannover Medical School
Andrej Kral
Hannover Medical School

Research Article

Keywords: cochlear geometry, cochlear anatomy, cochlear implantation, perimodiolar arrays

Posted Date: July 22nd, 2021

DOI: https://doi.org/10.21203/rs.3.rs-688018/v1

Variations in Microanatomy of the Human Modiolus: Implications for Cochlear Implants

Markus Pietsch[1,2,3*], Daniel Schurzig[1,3,4*], Rolf Salcher[1], Athanasia Warnecke[1], Peter Erfurt[1], Thomas Lenarz[1], Andrej Kral[1,3,5]

[1]Dept. of Otolaryngology, Hannover Medical School, Hannover, Germany
[2]Dept. of Otolaryngology, Helios Clinic Hildesheim, Hildesheim, Germany
[3]Dept. of Experimental Otology, Hannover Medical School, Hannover, Germany
[4]MED-EL Research Center, Hannover, Germany
[5] Dept. of Biomedical Sciences, Faculty of Medicine and Health Sciences, Macquarie University, Sydney, Australia

* Contributed equally to the study

Short Running Head: Modiolar Interindividual Variability

Keywords: cochlear geometry, cochlear anatomy, cochlear implantation, perimodiolar arrays

Conflict of Interest: Dr. Daniel Schurzig is also a MED-EL employee.

Emails for correspondence:
markus.pietsch@helios-gesundheit.de
schurzig.daniel@mh-hannover.de
salcher.rolf@mh-hannover.de
warnecke.athanasia@mh-hannover.de
lenarz.thomas@mh-hannover.de
kral.andrej@mh-hannover.de

Abstract

Human cochlear anatomy is highly variable. The phenomenon has been first described qualitatively, followed by a quantitative variability assessment with detailed anatomical models of the human cochlea. However, all previous work focused on lateral cochlear wall. Few information is available on the variability of the modiolar wall. Modiolar variability, likely determined by variability in the spiral ganglion, provides key information on when during ontogenesis the individual cochlear morphology is established: before and/or after neuronal structures are formed. In the present study we analyzed 108 corrosion casts, 95 clinical cone beam computer tomographies and 15 µCTs of human cochleae and observed modiolar variability of similar and larger extent than the lateral wall variability. Lateral wall measures correlated with modiolar wall measures significantly. ~49% of the variability has a common cause, very likely established already during the time when the spiral ganglion is formed. Proximity of other neuronal and vascular structures, defining the remaining variability in scalar spaces, are determined later in ontogenesis, when the scalae are formed. The present data further allows implications for perimodiolar cochlear implants and their tip fold-overs. In particular, the data demonstrate that tip fold-overs of preformed implants likely result from the morphology of the modiolus (with radius changing from base to apex), and that optimal cochlear implantation of perimodiolar arrays cannot be guaranteed without an individualized surgical technique.

Keywords:

Modiolus, variability, tip fold-over, efficient packing, implantation trauma.

Introduction

The shape of the human cochlea has an intriguing three-dimensional geometry that is reminiscent of the shell of a nautilus which remarkably fits to a logarithmic spiral [1–3]. A relation of the cochlear form to an acoustic function has been proposed [4]. The suggestion, however, is neither compatible with the overall size [5–10] nor the large interindividual variability of the cochlear shape (analysis in [8]). The Pietsch-data were compatible with the efficient packing hypothesis [11,12], assuming that the anatomical space restriction in the temporal bone, given by the proximity of nerves, muscles and vessels (embryonically forming before the cochlear spaces [13]), affects the interindividual variability in the cochlear shape. The shape was not compatible with a nautilus-like logarithmic spiral, but rather fits to a more complex polynomial spiral ([8], comp. [14]).

Human cochlear variability is of key importance for cochlear implantation. Implantation trauma and postoperative hearing outcomes are dependent on the mutual relation of cochlear size and the implant electrode [15–17]. Furthermore, variability in the vertical trajectory of the implant electrode can cause damage to the basilar membrane [7,18]. In these studies the vertical profile and the dimension of the scala tympani was less variable near the modiolus. Such an observation would favor perimodiolar electrodes [19–21], particularly since reduced distance to the modiolus may reduce channel interactions and reduce thresholds [22–24]. However, implantation trauma may be a serious complication [25–28]. Damage to the modiolus leads to loss of spiral ganglion cells [29] and may represent a route for infections into the intrathecal space [30]. Furthermore, perimodiolar placements require preformed electrode arrays [20,23]. These cannot be implanted in their precurved form, and even using a positioner (straightener or stylet) that straightens their form for implantation still involves the risk of a fold-over of the electrode array once it is released from the positioner [20,31–33] or a scalar translocation [34]. No detailed analysis of the relation between the electrode and the modiolus and its interindividual variability has been published yet. Knowledge on cochlear anatomy and its individual variations is of key importance for cochlear implantations of perimodiolar arrays.

Furthermore, it has been suggested that cochlear variability is due to the facial nerve, jugular vein, internal carotid and the tensor tympani muscle that are in close proximity of the cochlea and that form before the cochlear scalae [8]. The modiolus is ontogenetically formed before cochlear scalae [13]. Therefore, studying the modiolus in its interindividual variability would provide information whether developmentally, variability is established during cochlear spaces formation, or before their appearance. The latter would indicate that the formation of neural structures (that are the early structural basis of the modiolar geometry) is responsible for a substantial amount of cochlear variability.

The goal of the present study was to evaluate the variability of modiolar parts of the cochlea and compare it to the variations observed with measures obtained from the lateral wall. Three groups of specimen were compared: corrosion casts [8], micro computer tomography (µCT) datasets [35] and clinical measurements obtained with cone beam computer tomography (CT) in a clinical setting ([36]. The data show that the variability in cochlear microanatomy is similar in modiolar and lateral portions of the cochlea. The data presented allows for conclusions on current design issues of perimodiolar arrays.

Materials & Methods

Three different datasets of human cochlear anatomy were used in the present study: cone beam CT (CBCT) obtained in clinical setting before cochlear implantation (Fig. 1A), corrosion casts from donors (Fig. 1B) and micro-CTs (µCTs) from donors (Fig. 1C). While CBCT can be obtained in living human subjects, both corrosion casts and µCT are obtained from cadaver temporal bones. We have obtained informed consent from patients for using their data. All experimental protocols were approved by a institutional ethics committee at Hannover Medical School. All methods were performed in accordance with the relevant guidelines and regulations.

CBCT measurements ("Clinical CT")

The method of CBCT imaging and analysis and the dataset have been described in detail previously [36–38]; here we reuse these data. In brief, a total of 95 patients (51 female, 44 male) with cochlear implants were included in the analysis. The age of the patients ranged between 2 and 83 years (mean 54.3 yrs). All patients were treated at the Department of Otorhinolaryngology—Head and Neck Surgery of Hanover Medical School. Clinical CT images are anonymized. Segmentations were performed in clinical CBCT datasets acquired prior to surgery. CBCT datasets were generated using the Xoran XCAT (125 kVp, 7 mA) resulting in an isotropic voxel size of 0.3 mm or the Morita 3D Accuitomo 170 set to an isotropic voxel size of 0.08 mm.

These clinical scans are part of the clinical routine at the Hannover Medical School to preoperatively evaluate the condition of the cochlea and postoperatively confirm correct intracochlear array placement. All segmentations of the cochlear modiolar wall in preoperative CBCT data were performed with the software tool OsiriXMD (version 2.5.1 64bit, Pixmeo SARL, Switzerland) according to previous studies [37–40].

For a standardized view, window width was set to 4600 Hounsfield Units (HU) and window leveling was set to 1095 HU. The modiolar wall was measured along the A and B axis according to the previously accepted guidelines [41].

µCT

The method used for 15 µCTs has been described in detail previously [38]. In brief, 20 anonymized µCT data sets generated by a SCANCO MicroCT 100 (version 1.1, SCANCO Medical AG, Switzerland) were processed. The scans were performed at 70 kVp and 114 or 88 µA with Al05 or Cu01 filtering, resulting in a voxel size of 10 x 10 x 10 µm. The data sets were loaded into a custom software tool specifically developed for accurate segmentation of the cochlea. The utilized custom-made segmentation tool was programmed in C++ [42] with the goal to maximize the accuracy of the segmented cochlear structures. The resulting segmentation data points were then processed and converted within three main steps, all of which were performed in Matlab (version 2011a, The MathWorks Inc., USA) according to [38]. The cochlear lumina including the modiolus were segmented with an angular step width of 22.5° which was proven to be sufficiently small to serve as the foundation of convergence studies during data evaluation. Correspondingly, also here A and B measurements were performed according to [41].

Corrosion casts

The method used for 108 corrosion casts of human cochleae (59 left, 49 right) has been described in detail previously [8]. In brief, very high resolution imaging (12µm/pixel) in precise reproducible cross-hair-laser-assisted positioned views (according to the Consensus Cochlear Coordinate System / CCCS [41]) of corrosion casts from the Hanover Human Cochlea Database were studied. Measurements of distances, angles and areas were performed with the microscope manufacturers analysis software in maximal magnification (Keyence VHX-600). Measurement of cochlear length was performed with ImageJ software (Image Processing and Analysis in Java, freeware, available at http://rsbweb.nih.gov/ij/), which was calibrated for the pixel resolution. 120 measurement points in each of the 108 cochleae resulted in 11324 total measurements due to 818 missing values, mainly because the measurement point exceeded the given cochlea (e.g. measures at 990° were only available in cochleae that reached this angular length, in smaller cochleae these measurements were not available).

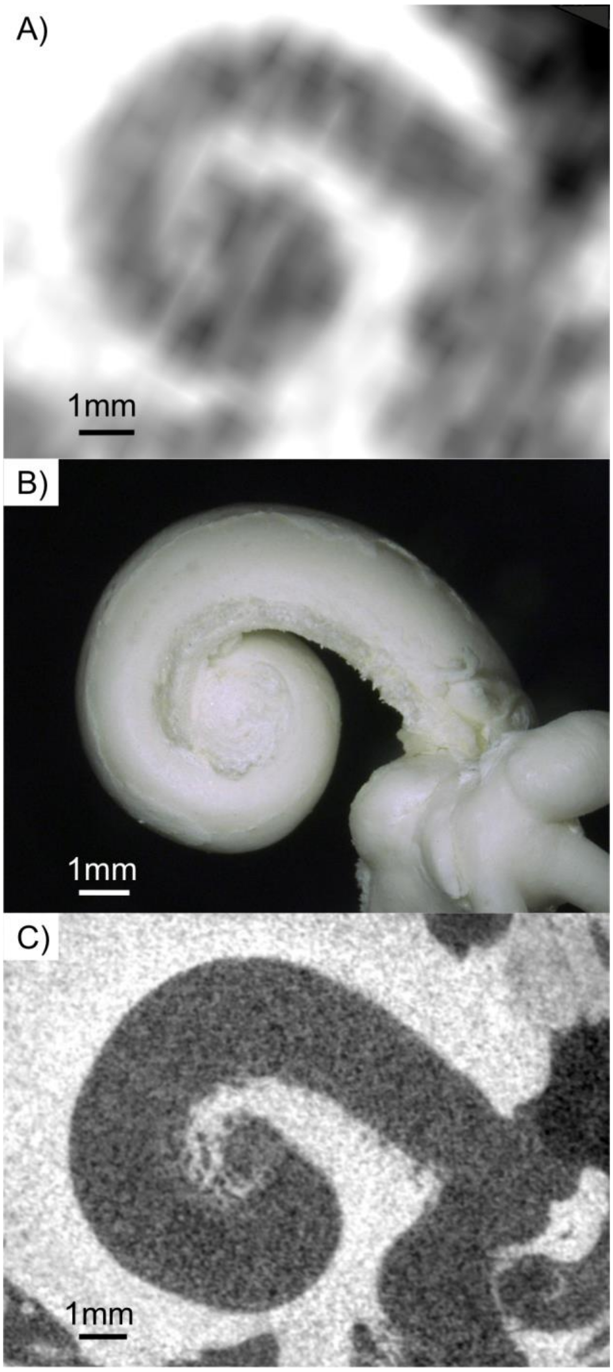

Figure 1: *Imaging of the cochlea using the three methods used in the present study: A) Cone Beam Computer Tomography (CBCT); B) Corrosion cast; C) Micro Computer Tomography (µCT). The different methods differ in resolution and details, with corrosion casts and µCTs providing better resolution than CBCT.*

Data analysis

The mean modiolar wall helix was computed based on the µCT data. First, the segmentation models of the 15 µCT datasets were averaged, yielding an average representation of the human cochlea. Based on this volumetric model the mean modiolar wall helix was extracted, as is depicted in Fig. 2A. The helix was then parameterized according to the ABH model [35], i.e. such that it could be scaled independently in x, y and z to match individual measures of the modiolar wall diameter A_{mod} and width B_{mod} (cf. Fig. 1B).

Individual cochlear diameter and width values for both the modiolar and lateral wall (Fig. 1B) were determined at the point where the porous modiolar wall transformed to the smooth scala tympani portion (Fig. 2B). These points at the A and B axis determined the A_{mod} and B_{mod}. The statistical analysis of all A and B measures [35,44] was performed in Matlab and significance was tested with two-tailed Wilcoxon-Mann-Whitney test and Kolmogoroff-Smirnoff test, both at α=5%.

For this analysis absolute values were compared, but additionally the values were normalized to the mean to assess the relative variance of the population. For this the values were normalized as

$$x_{norm} = \frac{x_1 \quad \bar{x}}{\bar{x}} \qquad \text{(Eq. 1)}$$

The A and B measures along the lateral and modiolar walls respectively were then used to scale the mean profiles of the two walls, yielding individual representations of the two walls for each cochlea. The analysis of the straight portion of the cochlear base and the critical diameters of the implant curvature was performed based on these individualized representations. The potential location of the cochlear implants (red curve in Fig. 2) was determined as a curve with an assumed constant offset (d_{off}) to the wall of the scala tympani (dashed line in Fig. 2C). Three commercial arrays with three different assumed d_{off} were modelled. The point of tangential transmission (Fig. 2C) was defined as the point where the tangent line to the position of the implant (dashed line) connects this point with the intersection of the A-axis and the lateral wall. This defined the angle of tangential transition $\Theta_{i,str}$ and the straight distance l_{str}.

Additionally, we studied the impact of modiolar variability on the risk of tip fold-over. In order to do so we introduced the critical radius r_{fold}, describing the curvature of an array tip small enough to enable the array to “stand up” on the modiolar wall (i.e. the critical radius that allows for a 90° angle between array tip and modiolar wall, as is depicted in Fig 2D; it is considered critical since an angle > 90° between array tip and modiolar wall will likely result in tip fold-over). Four values are hence important for the investigations described above: the distance of the electrode array to the modiolus (d_{off}, different for three different perimodiolar arrays), the minimal distance to the lateral wall (d_{LW}), the critical curvature of the preformed electrode array tip (r_{fold} in Fig. 2D) and the point of release of the electrode array from the stylet. We assumed three different distances from the modiolus based on three different electrode arrays (see results) and compared the resulting radius of the electrode tip (r_{pre}) with the critical radius (r_{fold}) at the given implantation angle in all 108 corrosion casts.

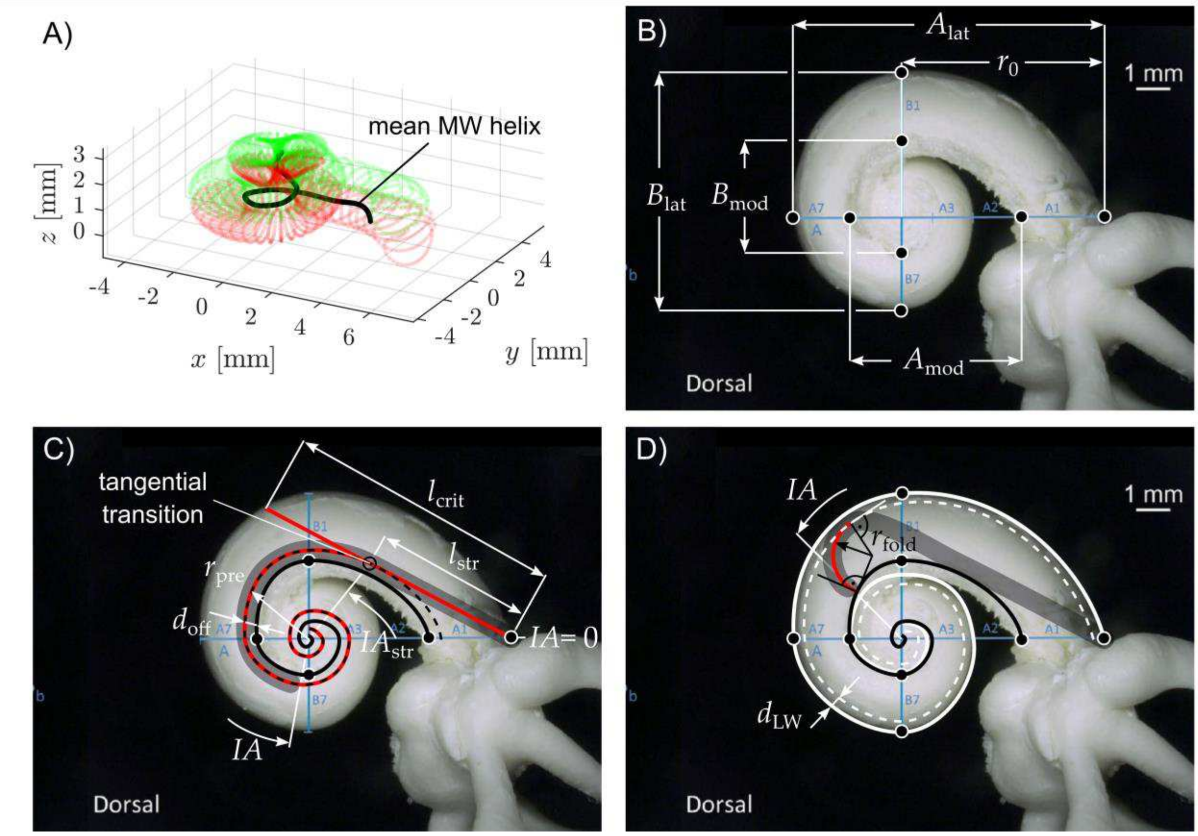

Figure 2: *The methodological approach. A) The average 3D profile of the cochlear MW extracted from the 15µCT segmentations described in [35]. B) Depiction of the cochlear dimensions A and B along the cochlear lateral and modiolar wall as well as the distance r_0 from the modiolar axis to the center of the round window; C) Visualization of the computed insertion trajectory (in red) based on the individualized MW profile (solid black line) and distance d_{off} between MW and central axis of a perimodiolar array. D) The computation of the critical radii (r_{fold}) were based on the assumption that if the radius of the precurved implant is small enough for the tip to "stand up" inside the scala tympani, a tip fold-over becomes likely. For this reason such hypothetical critical radius was computed depending on the different modiolar dimensions and different insertion angles.*

Results

Using the large dataset of more than 200 human cochleae obtained with different methods, we first focused on measures that can be easily obtained in all these approaches. Using such strategy it was possible to compare the different methods to each other and by that validate them.

The most straightforward comparison of variability was using the measures obtained at A and B axes of the cochlea in clinical CTs, µCT and corrosion casts. Comparing the three methods reveals that all measures taken at the lateral wall are similar and overlapping with these techniques (Fig. 3). The differences were systematic at the modiolar wall and, for B-axis, also at the lateral wall (A-values lateral wall: corrosion 9.24±0.42 mm; clinical 9.18±0.40, $p=0.2950$; A-values, modiolar wall: corrosion 5.46±0.32 mm; clinical 4.66±0.34 mm, $p=1.9961*10^{-29}$, B-values, lateral wall: corrosion 6.80±0.36; clinical 6.99±0.31; $p=1.0996*10^{-4}$; B-values, modiolar wall: corrosion 3.17±0.32, clinical 2.82±0.26, $p=2.1310*10^{-14}$, two-tailed Wilcoxon-Mann-Whitney test). The measures taken with µCT were too few in number to well characterize a histogram. They, nonetheless, overlapped with the range observed with the other two methods.

The measurements demonstrated systematic differences in the methods. The corrosion casts had a larger A compared to the clinical measurements, the B-results were mixed. Particularly the modiolar clinical measures appeared systematically smaller than the corrosion casts. This difference is likely given by the soft tissue at the cochlear base, since the measures taken with corrosion casts include soft tissue with the modiolar measurements, whereas the clinical CT and µCT visualize only the bone and exclude the soft tissue. These differences may have been further affected by the limited resolution of the clinical measurements. Most important for the present aim is, however, that the variance of the measures is highly similar for modiolar and lateral wall measures.

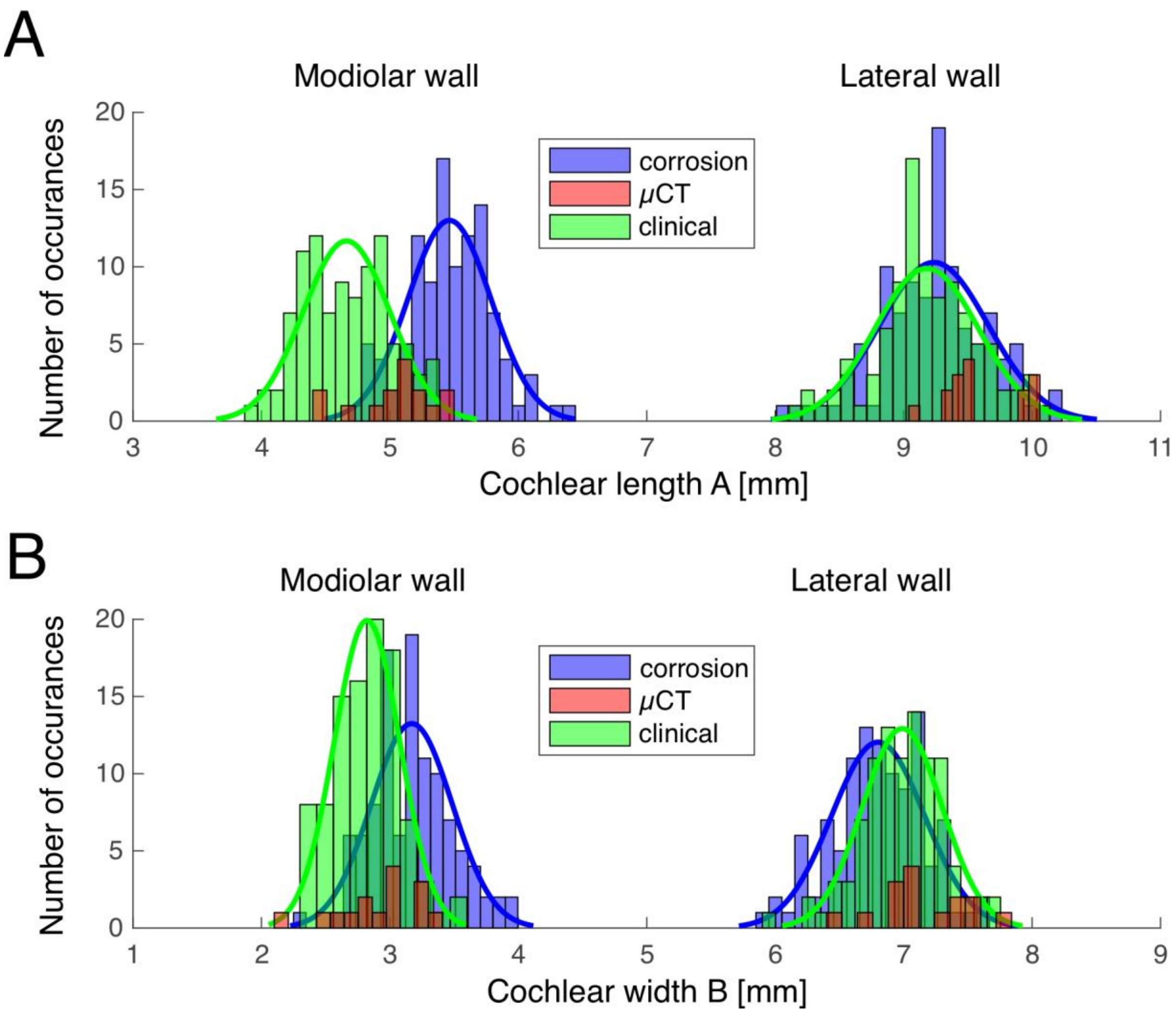

Figure 3: *Variability of A and B measures of the lateral wall and modiolar wall in the three datasets used.*

The coefficient of variation, relating the variance to the mean of the population and thus providing a quantification of the spread of the data, was nominally always larger, not smaller, for the modiolar measures: For the corrosion casts and the A-value, it was 0.0446 for the lateral wall and 0.0586 for the modiolar wall. For the B-value it was 0.0529 for the lateral wall and 0.1009 for the modiolar wall. Similarly, in the clinical measurements for the A-value, the coefficient of variation was 0.0436 for the lateral wall and 0.0730 for the modiolar wall. For the B-measure, it was 0.0443 for the lateral wall and 0.0922 for the modiolar wall. This indicates that the interindividual variability of the modiolar wall is not smaller than the variability of the lateral wall.

We subsequently analyzed the correlations between modiolar and lateral measures (Fig. 4). The values correlated significantly for all methods used. The best correlation was achieved for the corrosion casts (values of r ~0.7), where precision of measurement is likely highest. Not unexpectedly this indicates that the measurements taken from clinical CTs are confounded by some measurement imprecisions due to low contrast and resolutions. The µCT measurements were too few for this type of analysis, but even in these measurements the correlations were significant for the B values.

In the corrosion casts, the correlation explained approximately 49% of the variability of the modiolar measures by lateral measures (or vice versa). This means cochleae that are large in the lateral measures are also large in the modiolar measures. However, there is also variability in the size of the cochlear spaces, contributing to the “noise” in this correlation and probably contributing to the remaining 51% of the variability.

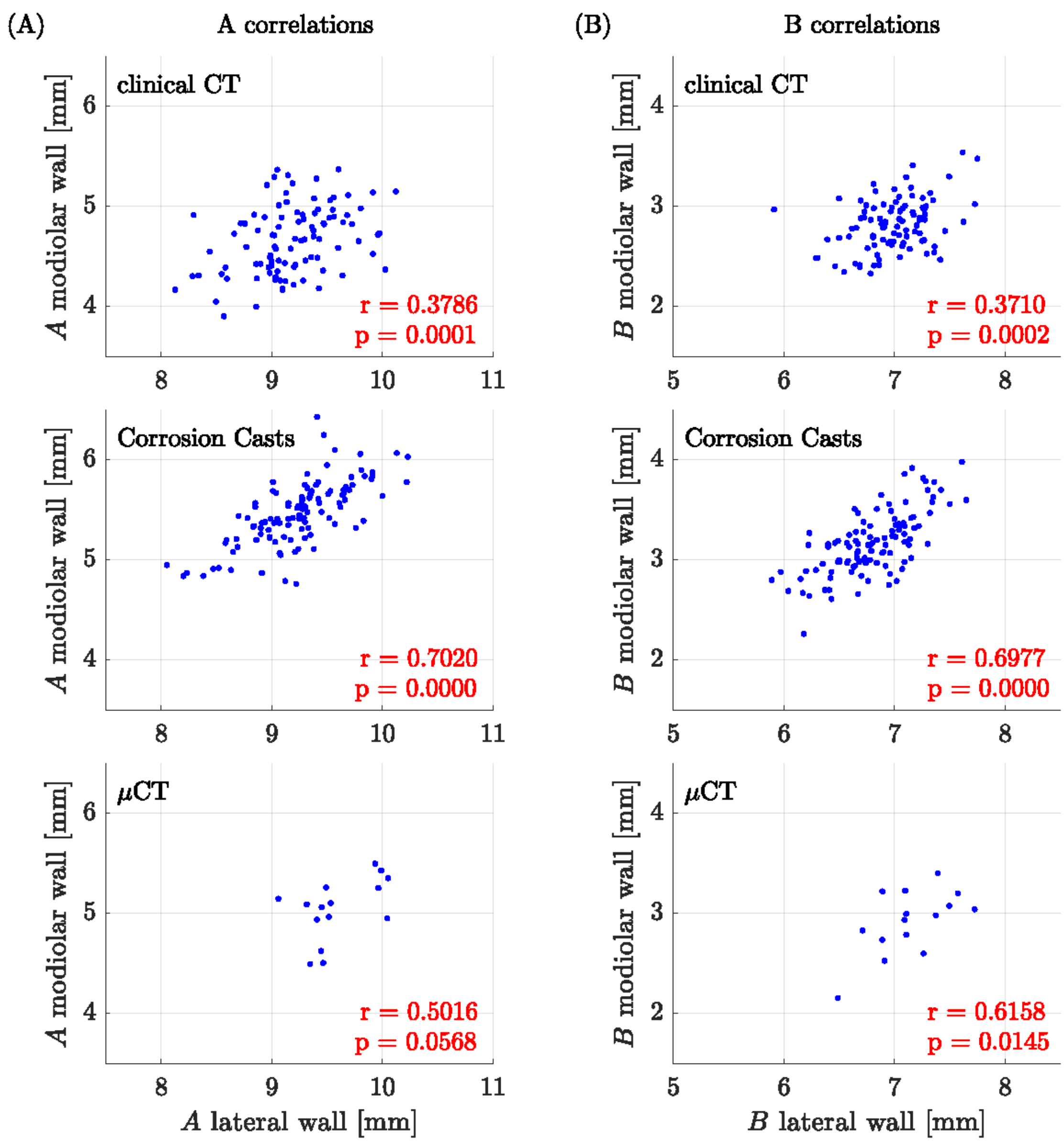

Fig. 4: *Correlations of (A) basal diameter A and (B) width B of the lateral and modiolar wall respectively, which were investigated for Clinical CT data (top row), Corrosion Casts (center row) and μCT (bottom row)*

Given these results, we normalized the distributions (subtracted the mean and divided by the mean, see Eq. 1) so that modiolar and lateral wall measures could be overlaid and directly compared (Fig. 5). This confirmed the surprising result: here the modiolar measures had in part larger variance than the lateral wall measures (Kolmogoroff-Smirnoff two-tailed test, $p<0.05$).

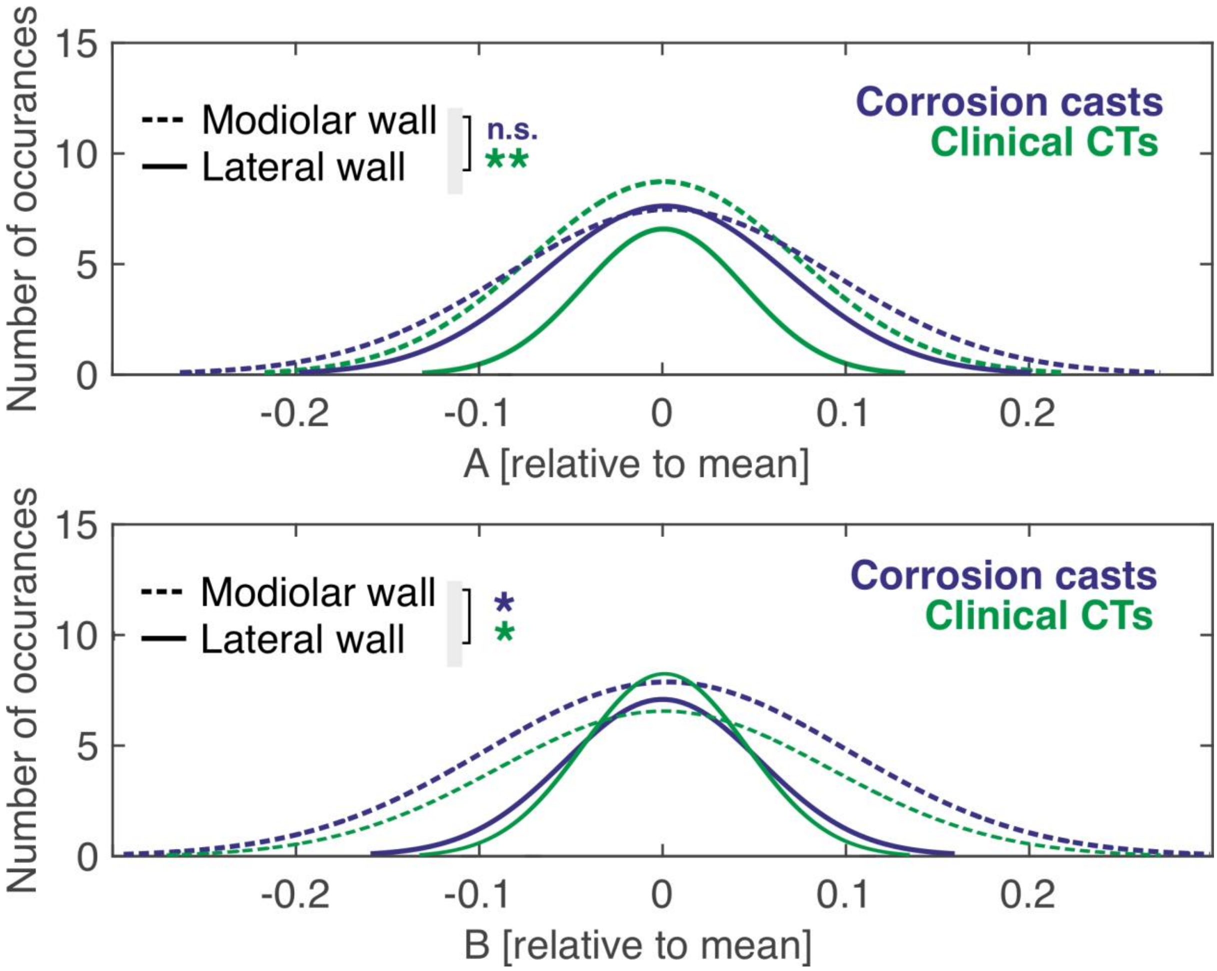

Fig. 5: *Comparison of the variance of lateral wall and modiolar wall measures after subtracting the mean and normalizing to the mean. * ~ p<0.05; ** ~p<0.01; n.s. = not significant ~ p>0.05.*

Finally, we also compared the measures between corrosion casts and the clinical CT measures: here the variance was not significantly different between the methods (modiolar wall A measures: p=0.2438; B measures: p=0.8527; lateral wall A measures: p=0.8431; B measures: p=0.4444).

Our data further allow a model-based assessment of the relation between the cochlear insertion depth (metric and angular) to the distance from the modiolus. The model was based on the corrosion cast data, being the largest sample in the present study at the highest spatial resolution. Using these data we can determine the angular insertion depth or insertion angle (*IA*) of an electrode as a function of the electrode insertion depth (*EID*) and the distance from the modiolus (d_{off}). We used this model to study the three currently most frequently used perimodiolar electrode arrays: the *Contour Advance electrode array* (CI612, Cochlear Ltd.), the *Mid-Scala electrode array* (HiFocus Mid-Scala, Advanced Bionics) and the *Slim Modiolar electrode array* (CI632, Cochlear Ltd.). These electrodes were all designed to come close to the modiolus and therefore modiolar variability is relevant for these implants. Furthermore, for all three electrodes, clinical insertion depths are available and can be compared to the outcomes of our estimations.

In order to tune our model to the different types of electrodes, we took the mean shape of the cochlear modiolar wall and computed the ratio of electrode insertion depth (*EID*) and resulting insertion angle (*IA*) for different values of d_{off} ranging from 0-1.5mm in 0.1mm steps. This computation yielded the three-dimensional profile depicted in Fig. 6 describing the average dependency of *EID*, *IA* and d_{off}. The 3D profile shows that for more modiolarly located electrode arrays, as expected, smaller *EID*s are necessary to achieve specific *IA*s. Using clinical observations on the mean ratio of *EID* and *IA* for the respective electrodes, the electrode-dependent value of d_{off} could be derived: the mean profile showed an *IA* of 348° with an *EID* of 16.6mm (as reported in [45] for the Contour Advance) for d_{off}=0.8mm, an *IA* of 398° with an *EID* of 19.2mm (as reported in [46] for the Mid-Scala) for d_{off}=1.0mm and an *IA* of 406° with an *EID* of 15.4mm (as reported in [47] for the Slim Modiolar) for d_{off}=0.3mm.

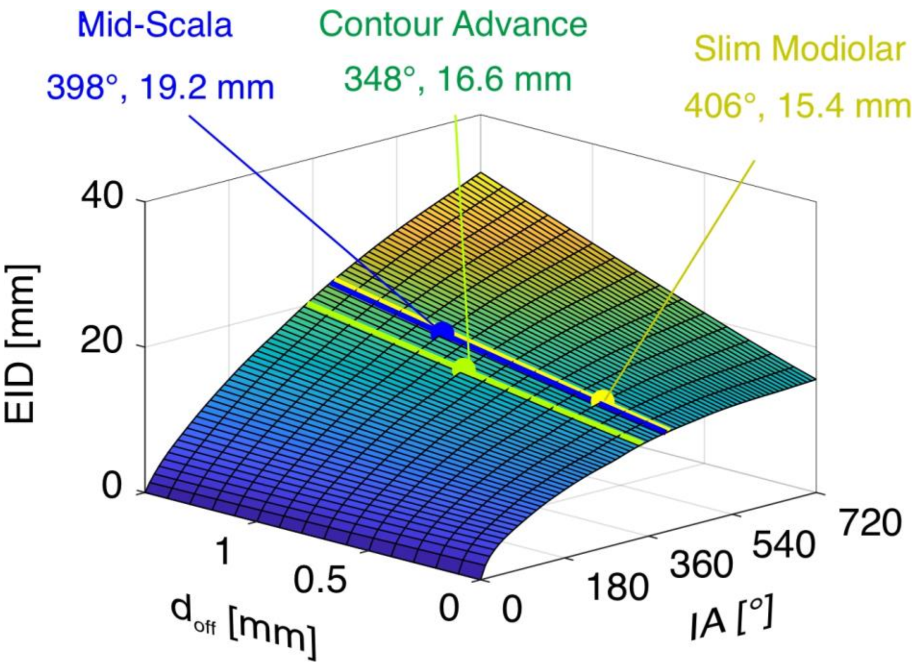

Fig. 6: *Dependence of the insertion depth (IED) to implantation angle (IA) on the distance from modiolus (d_{off}) of three different commercial perimodiolar electrode arrays. Data approximated based on an individual corrosion cast reflecting the mean overall size of the human cochlea. For same implantation angle shorter insertion depth is required if the distance to the modiolus is smaller.*

In order to validate if employing these offset values yields data on metric and angular insertion depth which is comparable to clinical observations we additionally took standard deviation data reported in the three publications on the respective perimodiolar arrays into account. Using the average shape of the modiolar wall we used the model to compute the metric insertion depth (*EID*) necessary to achieve the reported average insertion angles +/- 1 standard deviation of the respective electrode arrays. As shown in Fig. 7, the computed *EID* ranges necessary to achieve the clinically observed ranges of insertion angles are very similar to the ones assessed within clinical data: for the Contour Advance electrode the mean implantation angle of 348 ± 36° was clinically achieved with an EID of 16.6 ± 1.1mm [45], the model prediction was nearly identical - 16.7 +/- 1.1mm (Fig. 7ü). For the Mid Scala electrode, clinical data have shown that the mean implantation angle of 398 ± 41° required an EID of 19.1 ± 0.9 mm [46] and the model prediction was again nearly identical - 19.2 ± 1.3mm (Fig. 7). For the Slim Modiolar electrode, clinical observations showed a mean insertion angle of 406 ± 33° with an EID of 15.4 ± 1.1 mm [47] while the model predicted that these insertion angles can be achieved with an IED of 15.43 ± 0.06 mm.

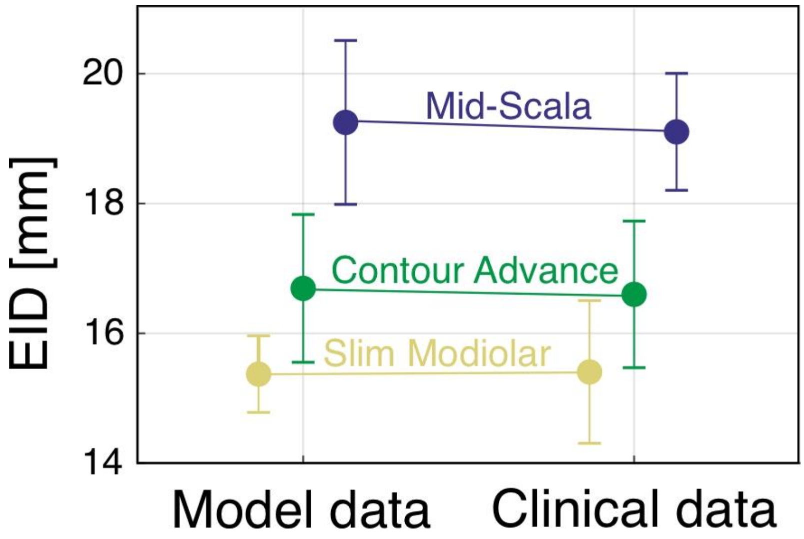

Fig. 7: *Comparison of model computations with previously published data on EID confirm the validity of the approximation based on corrosion casts, with nearly identical means and standard deviations. Clinical data for Contour Advance from [45], Mid-Scala electrode from [46] and Slim Modiolar from [47].*

After this validation step the model was used to investigate the insertions of perimodiolar arrays which follow the trajectories of commercial electrode arrays (due to the correspondingly matched d_{off} values of 0.3 mm, 0.8 mm and 1.0 mm) in more detail. This was performed by computing the relation of metric and angular insertion depths, i.e. what *EID* values are necessary to achieve specific *IA*s, for each one of the 108 cochleae with each one of the different values of d_{off}. It is important to note that these results are theoretical predictions based on the electrode shape and the corrosion casts.

The first critical measure of the insertion of perimodiolar arrays is the length of the straight portion of the implant in the basal cochlear turn. This measure is highly variable and dependent on the position of the electrode array within the scala tympani. The distance l_{str} and angle IA_{str} after which the array passes the tangential point and thus may be safely released from its straightener (Fig. 8A,B) varies substantially for the electrode distance from the modiolus (d_{off}). Thus l_{str} and IA_{str} are strongly dependent on the individual cochlear anatomy. The same holds true for the distance l_{crit} after which the array would touch the lateral wall, potentially causing insertion trauma (if not yet released from the straightener). The results show that the three investigated offsets d_{off} result in different l_{str}, IA_{str} and l_{crit}, i.e. all three parameters are not only dependent on the individual anatomy but also on the distance from the modiolus.

Interestingly, the ranges for the optimal release point l_{str} and the ranges critical for contacts with the lateral wall l_{crit} overlapped for d_{off} 0.8 and 1.0 mm. This demonstrates that for these distances from the modiolus there is no universally safe l_{str} that guarantees both (i) a safe release from straightener (without tip fold-over) and (ii) no risk of trauma at the lateral wall. In other words there is no “value that fits all” and the surgeon’s guides for release from stylet require at least different values for small, mean and large cochleae. This highlights again the importance of individually assessing the patient anatomy prior to implantation.

Next, the interrelation of *EID* and *IA* was investigated for the different values of d_{off}. The data, consistent with Fig. 6, further suggest that if an array is located closer to the modiolus, shorter insertion depths are required to achieve specific insertion angles (Fig. 8C). Modiolar electrodes of a certain length can thus theoretically achieve higher insertion angles than lateral wall electrodes of the same length. Pragmatically, these pre-curved electrodes are never inserted beyond or even up to 540°, which is most likely owed to the complexity of the insertion and trajectory the array must follow: the implantation with the stylet (in the straightened form) can only take place within the straight portion of the basal turn (l_{str}). Afterwards the implant has to be released and proceeds through the cochlea in its predetermined curvature which, if not coinciding with the curvature of the cochlea it is inserted into, would increase the risk of tip fold-overs (which is investigated in more detail below). In order to highlight the increasing complexity of the necessary array trajectory for deep, perimodiolar insertions, the median trajectories for angular insertion depths of 720° are depicted underneath Fig. 8C. These suggest that especially for a very close proximity to the modiolus, the array needs to be very tightly twisted. In addition, the pre-curvature can no longer be two-dimensional but must incorporate the height change of the cochlear spiral. This further increases the risk of basilar membrane puncture in the base as the coiling force would likely be applied directly upwards against the membrane.

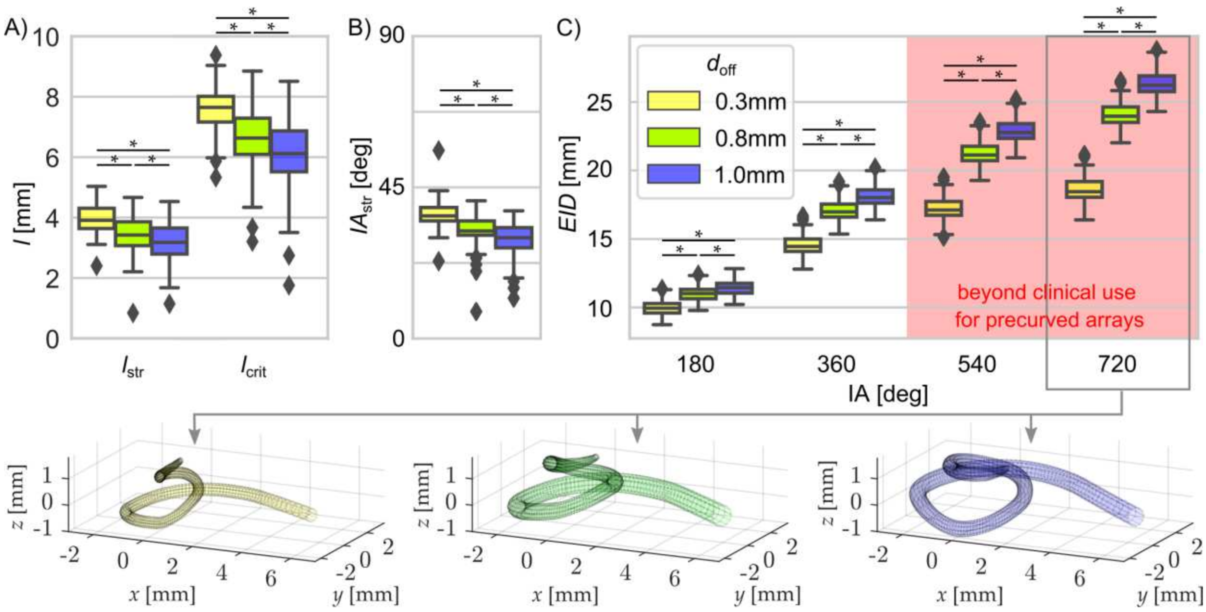

Figure 8: *Approximated position of the cochlear implant array for three conventional perimodiolar electrodes with different distance to the modiolar wall. Shown are theoretical values; perimodiolar or midscala arrays were not designed for the implantation of 540° or beyond. A) The straight portion of the cochlear implant as well as the critical distance at which the straight portion would touch the lateral wall are largest for the electrode that is closest to the modiolus. B) Also the implantation angle covered by the straight portion of the implantation is largest in the electrode that is closest to the modiolus. C) Relation of insertion depth (in mm) as a function of implantation angle. The electrode that is closest to the modiolus (Slim Modiolar) theoretically requires shorter electrode array to reach the end of the second turn. The median trajectories for an insertion angle of 720° shown below suggest that close proximity to the modiolus requires a more complex array 3D curvature, which is likely to increase the risk of tip fold-over.*

In order to further quantify the risk of tip fold-overs, we analyzed the critical radii (i.e. the maximal curvatures of pre-shaped arrays that involve the risk of tip fold-over by exceeding the 90° angle to the modiolar wall) in more detail. For this, in each individual corrosion cast the critical radii r_{fold} (as defined in Fig. 2D) were determined along the first two turns of the cochlea (Fig. 9). These values were highly interindividually variable. Nonetheless, within the first 270° the critical radius functions were rather flat, with a maximum of the mean curve of 1.37 mm. This is of importance, since the release from the straightener (e.g. stylet in case of Contour Advance) must take place within the first 45°-90°, but preferentially after the end of the straight portion of the implant course, thus after ~ 5 mm insertion (Fig. 8B). In consequence, to safely prevent tip foldover at this position, the tip of the implant after release from the stylet should have a preformed radius ≥ 1.37 mm for the average cochlea such that the array tip cannot fold over within the basal cochlear region. However, the value of 1.37 mm is not optimal for all cochleae; to safely avoid tip foldover in all cochleae, the radius should even exceed 2 mm.

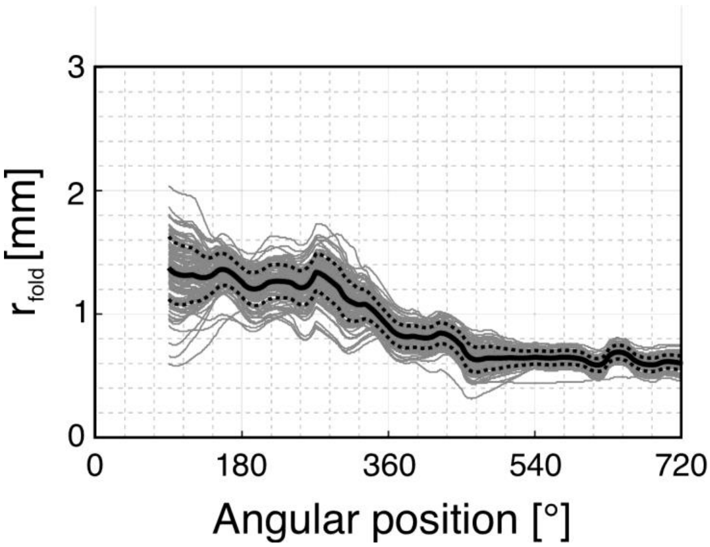

Figure 9: *The critical radii (r_{fold}) as determined from the 108 corrosion casts. The data reveal a rather flat function till 270°, with mean value of 1.37 mm and maximum values of up to 2.0 mm within the basal cochlear region. Around angular positions of 360°, the critical radii decline to < 1 mm.*

Since the modiolus becomes thinner in the apical direction, to come optimally close to the modiolus and remain closely positioned to the modiolus throughout the whole cochlea, the implant requires a particular radius (r_{pre}) at each angular position. This curvature is dependent on the assumed distance of the array from the modiolus. The next question was if this characteristic of critical radii r_{fold} can be compared with the curvatures r_{pre} of different electrode arrays (cf. Fig. 2) to derive array specific statements on increased risks for tip fold-overs. We assessed these hypothetical best curvatures for the three above approximated distance values d_{off} of 0.3 mm, 0.8 mm and 1.0 mm, which correspond to the commercial electrode arrays Slim Modiolar, Contour Advance and Mid-Scala, respectively, up to the first quadrant of the second turn. Fig. 10 hence shows the mean ± one standard deviation of the corresponding curvatures r_{pre} for which our model computes insertion angle comparable to clinical findings (Fig. 7). In addition, the mean profile of the critical radius r_{fold} ± one standard deviation as well as the maximum of the average critical radius of r_{fold} = 1.37 mm (dashed horizontal line) are displayed. Regarding the pre-curvature, all three array trajectories suggest decreasing r_{pre} profile (i.e. an increasing curvature) with increasing insertion angles as a consequence of the spiral profile of the cochlea with decreasing modiolar diameter. The different offsets d_{off}, representing the different proximities to the modiolar wall, mainly create a vertical shift of this curvature profile. The consequence of this shift regarding the chance of tip fold-overs can now be derived if comparing the curvature profiles with the dashed horizontal line (representing the projection of the average critical radius r_{fold} in the cochlear base, occurring at about 270°, array independent) onto the array dependent curvature profiles. All 3 comparisons show an intersection of the dashed line with the curvature profiles, and the angular value at which this intersection occurs (red arrow) is of critical importance. When starting with the array with medium distance from modiolus (0.8 mm, depicted in Fig. 10B), the figure shows the intersection of the two curves at about 380° (red arrow in Fig. 10B), which lies within the range of clinically reported insertion angles with the Contour Advance array. This means that the tip curvature of this array necessary to achieve the desired perimodiolar location at 380° equals the curvature which increases the likelihood of tip foldovers at 270°. In other words if releasing such a hypothetical array (designed so that its curvature fits optimally to the 380° point) from the straightener before or at the 270° point might yield a tip fold-over.

The more extreme case is the smallest distance from the modiolus (0.3 mm, Fig. 10A): the intersection of critical and pre-curvature radii lies on the top of the pre-curvature profile at 270°. The change of tip fold-overs is hence even larger than for

0.8 mm, since the tip curvature yielding the desired perimodiolar position and an increased chance of tip fold-overs are identical at 270° (bottom left illustration of Fig. 10). The diagram in Fig. 10A further shows that after about 500°, the pre-curvature radius r_{pre} is even smaller than the foldover critical radius r_{fold}. Foldovers beyond insertion angles of 500° are hence nearly inevitable with such array design.

In the other arrays (Fig. 10B,C) the mean optimal curvature is always above the critical curvature and this danger is consequently less (N.B. this applies for the mean cochleae only). This demonstrates that for assuring atraumatic insertion without the risk of tip fold-over, the electrode should be designed to be located more than 0.3 mm away from the modiolus.

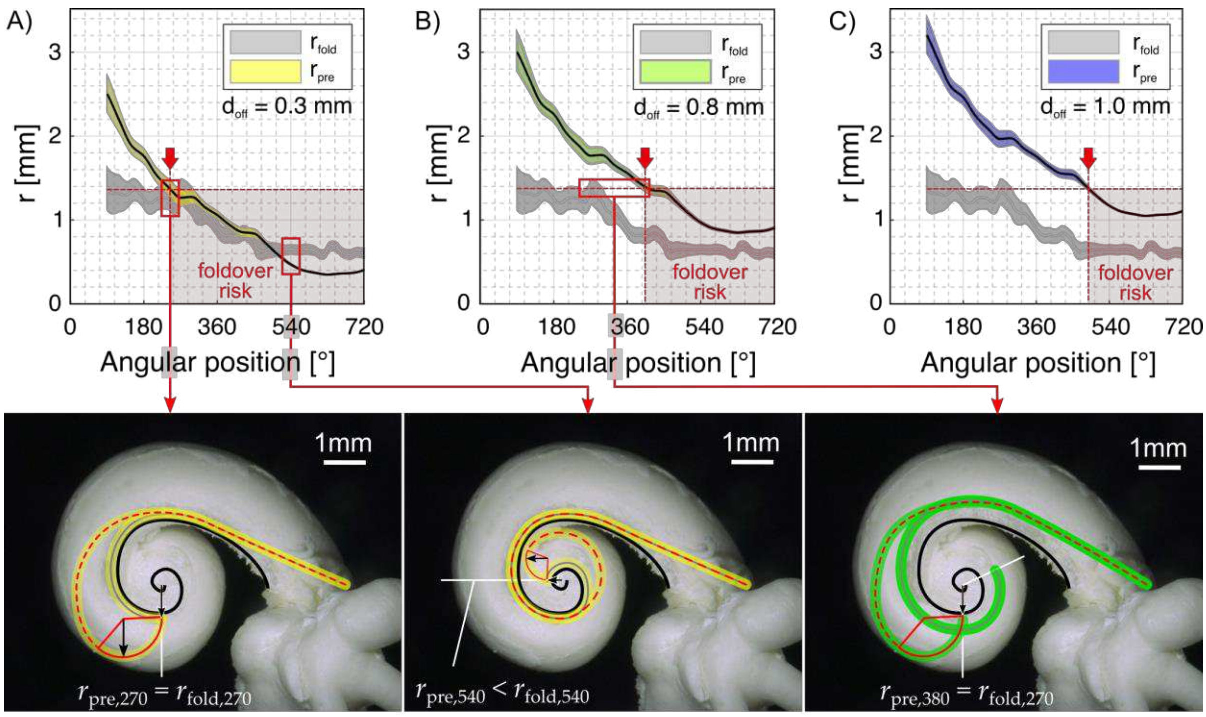

Fig. 10: *Mean (± standard deviation) of optimal radius (r_{pre}, i.e. optimal curvature of the preformed implant) as a function of angular position from the round window for the three different designs of the implants, with three different assumed distances from the modiolus (A: 0.3 mm; B: 0.8 mm and C: 1.0 mm). For comparison, mean values for the critical radius are shown in grey. Data obtained from corrosion casts. The red line depicts the maximal critical mean radius of 1.37 mm (occurring at about*

270°). The red arrow points to the angular position at which this line intersects the individual optimal array curvatures. Beyond this point this curvature would lead to an increased risk of foldovers because it allows the array tip to buckle up on the modiolus (see Fig. 2A). The bottom images show examples of (from left to right) desired and critical curvature occurring at the same angular location, the danger of the critical radius being even larger than the desired array radius and the desired curvature at an angle beyond 360° yielding an increased risk of tip foldovers within the basal turn.

It remains to be considered that mean r_{pre} values were used for the present considerations. However, these are highly variable between individuals, and only near the apex the variability is less – as shown by the minimal standard deviation in Fig. 10 for the highest implantation angles.

Discussion

The presented data provide evidence that the modiolar cochlear structures are either as variable as the cochlear lateral wall or, in some measures, even more variable than the lateral wall. In no case the variability of the modiolar walkl was less than that of the lateral wall. The interindividual variability of the human cochlea thus extends also into the modiolus that is, in contrast to the scalar spaces, primarily shaped by the early-developing neural structures.

The mechanistic explanation of cochlear variability has been so far based on the efficient packing hypothesis and the fact that scala vestibuli and scala tympani form after the differentiation of the surrounding neuronal structures. Since the present study did not assess neuronal structures directly, it cannot exclude the possibility that the neuronal structures are not variable and that only the scalar spaces approach them much closer in the smaller cochleae. This is, however, unlikely: the spiral ganglion is located extremely close to the scala tympani, the separation being only by a thin bony shell and sometimes a vessel (Fig. 9 of [48] and Fig. 6 of [49]; see also [50]). Therefore, interindividual differences in the modiolar axes must involve variations in the 3D shape of spiral ganglion. Indeed, also in a previous study metric length of the first two turns of the cochlea explained 83% of the variability of spiral ganglion length ([7], see also [51]). Most likely, it is already early in development when this part of the variability is established, before the scalar spaces appear. This suggests another an inherent source of variability of the cochlear size, potentially related to the overall size of the temporal bone and thus the size of the head that is additional to the efficient packing.

Methodologically, when comparing the lateral wall and the modiolar wall we need to consider that the borders of the lateral wall are much better defined in all imaging techniques. The modiolar wall is fenestrated, and thus the border is harder to identify than the lateral wall (Fig. 1). One can assume that the outcomes of modiolar measurements will be more affected by measurement imprecisions (noise) than at the lateral wall. This may have substantially contributed to the larger spread of the data for the normalized modiolar distributions compared to lateral wall (Fig. 4). The interesting finding is, however, the high correlation (r ~ 0.7) of both measures in corrosion casts (with the best spatial resolution, Fig. 3A,B). This demonstrates that the results in corrosion casts are not driven by measurement "noise" (that would be uncorrelated), but rather by true variability behind the data. Such common factors explain 49% of the variability of lateral and modiolar dimensions. Of key importance is the use of several techniques: here clinical CT was much more contaminated by such uncorrelated noise, and consequently the r values were smaller, ~ 0.37. Interestingly, where measurements can be performed exactly, in µCT, despite few data, correlation coefficients are higher than in clinical CTs (Fig. 4).

The modiolar A and B values were smaller in clinical CT than in corrosion casts, most prominently for measure A, but observable also for B. The µCT measurements were positioned in between. The CT measures reflect the bony structures and exclude soft tissue near the modiolus and the lateral wall, whereas the corrosion casts in fact show only the empty spaces and as a negative image include, particularly in the modiolar measures, the soft tissue. Additionally to the imprecisions in the assessment of the modiolar wall also this may further contribute to these differences.

Clinical implications

We investigated the consequence of the modiolar variability on the cochlear implantation. We have focused on three arrays that cover a wide range of distances from the modiolus. The present data confirm that compared to lateral wall arrays, perimodiolar implants of the same length have the potential to reach deeper into the cochlea. However, this includes risks in cochlear trauma and comes at a cost of a complex design that currently does not allow deep implantation (see also below): since the implant must be preformed, implantations require a stylet (or straightener).

Furthermore, perimodiolar arrays require a precurved geometry. A precurved electrode arrays often have a constant curvature along the array – in other words they are optimally designed for one insertion position (r_{pre} curves in Fig. 10). Before (basally to) this position the curvature will be smaller than optimal and even may be smaller than the critical radius (with the consequence of tip fold-over). Beyond this point (apical to it) it will be too large and thus come to lie further abmodiolarly, at an intermediate position between the modiolar and the lateral wall (comp. [52]).

Two additional anatomical limiting factors for perimodiolar electrodes require consideration:

1) The acceptable straight portion of implant course varied in different cochleae. The individual optimal straight insertion depth covers a range from 2 to 5 mm (Fig. 8B) depending on the microanatomy of the individual cochlea. The stylet itself can cause a cochlear trauma if inserted so deeply into the cochlea that it hits the lateral wall. The range of distances from round window straight to the lateral wall (along the course of l_{str} in Fig. 2) in the present study was 6.86 – 9.37 mm. The surgeon's guide for the Contour Advance electrode informs that the electrode tip is 7.6 mm from the marker for optimal insertion. This is > 0.7

mm more than the corresponding space in the smallest cochlea (Fig. 8 B). This means that this electrode would introduce cochlear damage at the lateral wall in smaller cochleae before the stylet is removed (albeit this is the case only in few cochleae; see also [53]). For the Slim-Modiolar electrode array the literature provides the information of "about 5 mm" insertion before straightener removal [54] and the Surgeon's guide for the Mid-Scala gives 5.4 mm (distance between marker and tip of the electrode). These two values appear to be the consequence of a reasonable safety consideration fitting to the mean values in Fig. 8B - it would be beyond the point where the straight electrode array passes tangentially the modiolus, but would still be ~ 1.86 mm before the lateral wall of the smallest cochleae. However, the more distant the electrode from the modiolus during straightener removal, the less space is available (Fig. 8B). Knowledge of the size of the straight distance (l_{str}) and the maximum length till lateral wall is touched allows for individualizing the implantation procedure; however, due to resolution of clinical CTs, use of cochlear models may be needed for assessing this parameter precisely [43].

2) The diameter of the modiolus decreases in the apical direction. The precurved diameter is dependent on the point where the release of the array from the stylet takes place (Fig. 10). The deeper the implantation, the smaller the diameter. At present, perimodiolar implants are mainly designed for implantation into the first turn. Nonetheless, higher cochlear coverage may provide more independent information channels and thus better speech understanding [17,55]. Thus, perimodiolar arrays always trade optimal position and risk of tip foldover.

The preformed implant should consider that apically the diameter of the curvature must be small to adhere to the modiolus in apical portions of the cochlea. This, however, may lead to tip fold-over if the release is taking place at the end of the straight portion of the implantation (after 45° implantation angle, Figs. 2, 8C and 9), where the critical radius is much larger than the hypothetical optimal curvature of the array tip. To prevent tip fold-over in this region, the preformed radius should exceed 1.37 mm. This, however, is larger than e.g. the curling radius of the Contour Advance electrode array [56]. The Contour Advance, likely in the intention to avoid this, has a conic straight silicone tip that extends for ~ 1 mm and is not curved. This is probably intended to lean on the modiolus and prevent a foldover. Nonetheless, even experienced surgeons cannot prevent tip fold-over in all cochleae with this electrode [20,32,33], indicating that this approach is not always successful.

This critical radius is too large for the more apical portions of the cochlea, where such curvature would again move the tip of the implant array away from the modiolus. This is in fact also observable in clinical analyses of the location of the cochlear implant in the human cochlea with modiolar-close and -distant portions of the array depending on the angular position [36,57]. Our data suggest that particularly implantations >400° would show the effect - the present day perimodiolar electrodes, fortunately, do not penetrate beyond this point into the cochlea.

Furthermore, at the border of the first and the second turn also a critical point of the vertical profile is observed in half of the cochleae (a vertical jump, [7]) that might further complicate such implantation. However, in perimodiolar positions the vertical profile was much smoother than in the lateral positions [7].

To optimize the implantation procedure and to exclude the risk of a tip fold-over, the present days electrode designs should aim at a distance to the modiolus of >0.3 mm or provide larger curvatures (>1.37 mm, best > 2 mm) after release from the straightener/stylet (Fig. 10). Clinical imaging outcomes of electrode array in use within the first cochlear turn show distances in the range 0.60 – 1.67 mm (for Cochlear 532/632 array 0.80±0.10 mm and for 512 array 0.76±0.07 mm; data from [58]). Closer locations, and thus true "modiolar hugging electrodes", particularly those aiming at implantations beyond 400°, require new surgical and technical approaches due to the changing diameter of the modiolus. Only electrodes that are implanted more laterally and subsequently approach the modiolus slowly, after the implant has been placed (e.g. by the increased temperature in the inner ear in implants integrating temperature-sensitive memory materials [59]) represent a viable approach for true modiolar-hugging electrodes extending beyond the first turn of the cochlea. Here, however, the approach to the modiolus should start basally and continue later apically to prevent that the implant is dragged out of the cochlea (which would occur if the process was opposite). Such approach may, however, involve a significant force on the modiolus, with associated risk of trauma. It is worth further investigations, given that modiolus-hugging electrodes in the past provided such excellent channel separation (in some patients) that multi-channel compressed analogue stimulation (providing temporal fine structure) could be clinically used [60]. Similarly, some studies indicate better speech perception with perimodiolar electrodes [61].

An interesting suggestion for achieving a better modiolar hugging position in the basal portion of the cochlea with current design of perimodiolar arrays is the "pull-back" technique [62,63]: after full insertion of the perimodiolar array the electrode is retracted back to eliminate buckling from the modiolus in the base. This might assure a better positioning in the base and does reduce the current spread [62].

Finally, the modiolar variability underscores the surgical challenges in trauma-free and fold-over-free implantations of perimodiolar arrays. The study strongly emphasizes the need of individualized implantation procedure for these arrays, with cochlear imaging and detailed planning using all methods available, including 3D cochlear models [43].

Cochlear variability beyond efficient packing

The present results also provide deeper understanding of the cochlear microanatomical variability and its reasons. Differences were noted in the extent of variability between A and B measures of the modiolus. Similarly, also in a previous study this has been described and has been interpreted as the facial nerve having a larger effect on the B axis of the cochlea compared to the internal carotid's effect on the A axis ([8], supplementary Fig. 4). Since modiolar variability is in fact larger than lateral wall variability, this suggests the action of at least two different factors.

While the present data are largely consistent with the efficient packing hypothesis [8], they call for an extension of the previous theory. We suggest the action of three independent factors in cochlear variability:

1) *Inherent variability* of the overall size of the cochlea affecting both the modiolar variability and lateral wall variability, a largely inherited factor. Both the A and B measures correlate with $r^2 = 0.64$ [8], and modiolar and lateral wall measures correlate with the same $r^2 = 0.49$ (present data). This together suggests that the inherent variability is responsible for the common ~ 50% of the

interindividual variations in all these measures and that it acts as a common background for all variations. Most likely it is the size of the skull base (temporal bone) that affects the overall size of the cochlea and is well observable in modiolar variability of B measure. This factor thus allows the cochlea to “grow larger”.

2) *Limiting factor* of neighboring structures, particularly facial nerve, as observed previously [8], is the second key player, potentially explaining the large part of the remaining variation ($1\text{-}r^2 = 0.51$). The action of this factor is stronger in extend at the B axis, where the closest structure, the facial nerve, is found. Proximity of the facial nerve limits the inherent variability of the lateral wall and causes this variability to be smaller than the modiolar variability. Limiting factors affect the growth involved in the inherent variability in some cochleae by preventing it “growing larger” along a specified direction. Such factors would be responsible for the complex, irregular geometry of the cochlea including dips, indentations and jumps in the form, as reported previously more prominently along the lateral wall [7,8].
3) *Measurement noise* that constitutes a part of the 51% mentioned in the *limiting factor* above. For modiolar wall, this imprecision is larger than for the lateral wall, the extent of it is, however, not clear.

These implications suggest that a correlation should be observed between head size and the cochlear size that explains the inherent variability (r^2=0.49). Unfortunately, the present clinical data do not include this information and therefore it requires future studies to test this hypothesis.

Acknowledgements

This work was funded by the Deutsche Forschungsgemeinschaft (DFG, German Research Foundation) under Germany's Excellence Strategy – EXC 2177/1 - Project ID 390895286.

Author contribution

MP, DS, and AK designed the study, MP and RS performed the measurements, DS analyzed the data, AK and DS prepared the figures and wrote the manuscript, all authors edited and approved it.

References

1. Erlich, A., Moulton, D. E., Goriely, A. & Chirat, R. Morphomechanics and Developmental Constraints in the Evolution of Ammonites Shell Form. *J Exp Zool B Mol Dev Evol* **326**, 437-450 (2016).
2. Chirat, R., Moulton, D. E. & Goriely, A. Mechanical basis of morphogenesis and convergent evolution of spiny seashells. *Proc Natl Acad Sci U S A* **110**, 6015-6020 (2013).
3. Marinković, S., Stanković, P., Štrbac, M., Tomić, I. & Ćetković, M. Cochlea and other spiral forms in nature and art. *Am J Otolaryngol* **33**, 80-87 (2012).
4. Manoussaki, D. et al. The influence of cochlear shape on low-frequency hearing. *Proc Natl Acad Sci U S A* **105**, 6162-6166 (2008).
5. Hardy, M. The length of the organ of Corti in man. *American Journal of Anatomy* **62**, 291-311 (1938).
6. Erixon, E., Högstorp, H., Wadin, K. & Rask-Andersen, H. Variational anatomy of the human cochlea: implications for cochlear implantation. *Otol Neurotol* **30**, 14-22 (2009).
7. Avci, E., Nauwelaers, T., Lenarz, T., Hamacher, V. & Kral, A. Variations in microanatomy of the human cochlea. *J Comp Neurol* **522**, 3245-3261 (2014).
8. Pietsch, M. et al. Spiral Form of the Human Cochlea Results from Spatial Constraints. *Sci Rep* **7**, 7500 (2017).
9. Helpard, L., Li, H., Rask-Andersen, H., Ladak, H. M. & Agrawal, S. K. Characterization of the human helicotrema: implications for cochlear duct length and frequency mapping. *Journal of Otolaryngology - Head & Neck Surgery* **49**, 1-7 (2020).
10. Helpard, L. W., Rohani, S. A., Ladak, H. M. & Agrawal, S. K. Evaluation of Cochlear Duct Length Measurements From a 3D Analytical Cochlear Model Using Synchrotron Radiation Phase-Contrast Imaging. *Otology & Neurotology* **41**, e21-e27 (2020).
11. Vater, M. & Kössl, M. Comparative aspects of cochlear functional organization in mammals. *Hear Res* **273**, 89-99 (2011).
12. Manley, G. A. Evolutionary paths to mammalian cochleae. *J Assoc Res Otolaryngol* **13**, 733-743 (2012).
13. Kopecky, B., Johnson, S., Schmitz, H., Santi, P. & Fritzsch, B. Scanning thin-sheet laser imaging microscopy elucidates details on mouse ear development. *Dev Dyn* **241**, 465-480 (2012).
14. Yoo, S. K., Wang, G., Rubinstein, J. T. & Vannier, M. W. Three-dimensional geometric modeling of the cochlea using helico-spiral approximation. *Biomedical Engineering, IEEE Transactions on* **47**, 1392-1402 (2000).
15. Holden, L. K. et al. Factors Affecting Open-Set Word Recognition in Adults With Cochlear Implants. *Ear Hear* **34**, 342-360 (2013).
16. Avci, E., Nauwelaers, T., Hamacher, V. & Kral, A. Three-Dimensional Force Profile During Cochlear Implantation Depends on Individual Geometry and Insertion Trauma. *Ear Hear* **38**, e168-e179 (2017).
17. Büchner, A., Illg, A., Majdani, O. & Lenarz, T. Investigation of the effect of cochlear implant electrode length on speech comprehension in quiet and noise compared with the results with users of electro-acoustic-stimulation, a retrospective analysis. *PLoS One* **12**, e0174900 (2017).
18. Jagt, A. M. A. V. D., Kalkman, R. K., Briaire, J. J., Verbist, B. M. & Frijns, J. H. M. Variations in cochlear duct shape revealed on clinical CT images with an automatic tracing method. *Sci Rep* **7**, 17566 (2017).

19. Hughes, M. L. & Abbas, P. J. Electrophysiologic channel interaction, electrode pitch ranking, and behavioral threshold in straight versus perimodiolar cochlear implant electrode arrays. *The Journal of the Acoustical Society of America* **119**, 1538-1547 (2006).
20. Briggs, R. J. S. et al. Development and evaluation of the modiolar research array - multi-centre collaborative study in human temporal bones. *Cochlear Implants Int* **12**, 129-139 (2011).
21. Ramos-Macías, A., Borkoski-Barreiro, S. A., Falcón-González, J. C. & Ramos-de Miguel, A. Hearing Preservation with the Slim Modiolar Electrode Nucleus CI532® Cochlear Implant: A Preliminary Experience. *Audiol Neurootol* **22**, 317-325 (2017).
22. Shepherd, R. K., Hatsushika, S. & Clark, G. M. Electrical stimulation of the auditory nerve: the effect of electrode position on neural excitation. *Hear Res* **66**, 108-120 (1993).
23. Friedmann, D. R., Kamen, E., Choudhury, B. & Roland, J. T. Surgical Experience and Early Outcomes With a Slim Perimodiolar Electrode. *Otol Neurotol* **40**, e304-e310 (2019).
24. Risi, F. Considerations and rationale for cochlear implant electrode design-past, present and future. *The journal of international advanced otology* **14**, 382 (2018).
25. Gstoettner, W. K. et al. Perimodiolar electrodes in cochlear implant surgery. *Acta oto-laryngologica* **121**, 216-219 (2001).
26. Eshraghi, A. A., Yang, N. W. & Balkany, T. J. Comparative study of cochlear damage with three perimodiolar electrode designs. *Laryngoscope* **113**, 415-419 (2003).
27. Wardrop, P., Whinney, D., Rebscher, S. J., Luxford, W. & Leake, P. A temporal bone study of insertion trauma and intracochlear position of cochlear implant electrodes. II: Comparison of Spiral Clarion and HiFocus II electrodes. *Hear Res* **203**, 68-79 (2005).
28. Roland Jr, J. T. A model for cochlear implant electrode insertion and force evaluation: results with a new electrode design and insertion technique. *The Laryngoscope* **115**, 1325-1339 (2005).
29. Leake, P. A., Hradek, G. T. & Snyder, R. L. Chronic electrical stimulation by a cochlear implant promotes survival of spiral ganglion neurons after neonatal deafness. *J Comp Neurol* **412**, 543-562 (1999).
30. Reefhuis, J. et al. Risk of bacterial meningitis in children with cochlear implants. *N Engl J Med* **349**, 435-445 (2003).
31. Grolman, W. et al. Spread of excitation measurements for the detection of electrode array foldovers: a prospective study comparing 3-dimensional rotational x-ray and intraoperative spread of excitation measurements. *Otology & Neurotology* **30**, 27-33 (2009).
32. Gabrielpillai, J., Burck, I., Baumann, U., Stöver, T. & Helbig, S. Incidence for Tip Foldover During Cochlear Implantation. *Otol Neurotol* **39**, 1115-1121 (2018).
33. Klabbers, T. M., Huinck, W. J., Heutink, F., Verbist, B. M. & Mylanus, E. A. M. Transimpedance Matrix (TIM) Measurement for the Detection of Intraoperative Electrode Tip Foldover Using the Slim Modiolar Electrode: A Proof of Concept Study. *Otology & Neurotology* **42**, e124-e129 (2021).
34. Jwair, S. et al. Scalar Translocation Comparison Between Lateral Wall and Perimodiolar Cochlear Implant Arrays - A Meta- Analysis. *The Laryngoscope* **131**, 1358-1368 (2021).
35. Schurzig, D. et al. Cochlear helix and duct length identification - Evaluation of

different curve fitting techniques. *Cochlear Implants Int* 1-16 (2018).
36. Salcher, R. et al. On the Intracochlear Location of Straight Electrode Arrays After Cochlear Implantation: How Lateral Are Lateral Wall Electrodes. *Otology & Neurotology* **42**, 242-250 (2021).
37. Schurzig, D., Timm, M. E., Batsoulis, C., John, S. & Lenarz, T. Analysis of different approaches for clinical cochlear coverage evaluation after cochlear implantation. *Otology & Neurotology* **39**, e642-e650 (2018).
38. Schurzig, D., Lexow, G. J., Majdani, O., Lenarz, T. & Rau, T. S. Three-dimensional modeling of the cochlea by use of an arc fitting approach. *Computer Methods in Biomechanics and Biomedical Engineering* **19**, 1785-1799 (2016).
39. Würfel, W., Lanfermann, H., Lenarz, T. & Majdani, O. Cochlear length determination using Cone Beam Computed Tomography in a clinical setting. *Hear Res* **316C**, 65-72 (2014).
40. Timm, M. E. et al. Patient specific selection of lateral wall cochlear implant electrodes based on anatomical indication ranges. *PLoS One* **13**, e0206435 (2018).
41. Verbist, B. M. et al. Consensus Panel on a Cochlear Coordinate System Applicable in Histologic, Physiologic, and Radiologic Studies of the Human Cochlea. *Otol Neurotol* **31**, 722-730 (2010).
42. Lexow, G. J. et al. Visualization, measurement and modelling of the cochlea using rotating midmodiolar slice planes. *Int J Comput Assist Radiol Surg* **11**, 1855-1869 (2016).
43. Schurzig, D. et al. A Cochlear Scaling Model for Accurate Anatomy Evaluation and Frequency Allocation in Cochlear Implantation. *Hearing Research* **403**, 108166 (2021).
44. Escudé, B. et al. The size of the cochlea and predictions of insertion depth angles for cochlear implant electrodes. *Audiol Neurootol* **11 Suppl 1**, 27-33 (2006).
45. Ketterer, M. C. et al. The influence of cochlear morphology on the final electrode array position. *Eur Arch Otorhinolaryngol* **275**, 385-394 (2018).
46. Hassepass, F. et al. The new mid-scala electrode array: a radiologic and histologic study in human temporal bones. *Otology & Neurotology* **35**, 1415-1420 (2014).
47. McJunkin, J. L., Durakovic, N., Herzog, J. & Buchman, C. A. Early outcomes with a slim, modiolar cochlear implant electrode array. *Otology & Neurotology* **39**, e28-e33 (2018).
48. Roland, P. S. & Wright, C. G. Surgical aspects of cochlear implantation: mechanisms of insertional trauma. *Adv Otolaryngol* **64**, 11-30 (2006).
49. Wright, C. G. & Roland, P. S. Vascular trauma during cochlear implantation: a contributor to residual hearing loss? *Otology & Neurotology* **34**, 402-407 (2013).
50. Li, H. et al. Three-dimensional tonotopic mapping of the human cochlea based on synchrotron radiation phase-contrast imaging. *Sci Rep* **11**, 4437 (2021).
51. Stakhovskaya, O., Sridhar, D., Bonham, B. H. & Leake, P. A. Frequency map for the human cochlear spiral ganglion: implications for cochlear implants. *J Assoc Res Otolaryngol* **8**, 220-233 (2007).
52. Lee, S.-Y. et al. Modiolar proximity of slim modiolar electrodes and cochlear duct length: correlation for potential basis of customized cochlear implantation with perimodiolar electrodes. *Ear and Hearing* **42**, 323-333 (2021).
53. Rebscher, S. J. et al. Considerations for design of future cochlear implant

electrode arrays: electrode array stiffness, size, and depth of insertion. *J Rehabil Res Dev* **45**, 731-747 (2008).

54. Aschendorff, A. et al. Clinical investigation of the Nucleus Slim Modiolar Electrode. *Audiol Neurootol* **22**, 169-179 (2017).
55. O'Connell, B. P. et al. Insertion depth impacts speech perception and hearing preservation for lateral wall electrodes. *Laryngoscope* **127**, 2352-2357 (2017).
56. Rau, T. S., Majdani, O., Hussong, A., Lenarz, T. & Leinung, M. Determination of the curling behavior of a preformed cochlear implant electrode array. *Int J Comput Assist Radiol Surg* **6**, 421-433 (2011).
57. Finley, C. C. et al. Role of electrode placement as a contributor to variability in cochlear implant outcomes. *Otol Neurotol* **29**, 920-928 (2008).
58. Degen, C. V., Büchner, A., Kludt, E. & Lenarz, T. Effect of Electrode to Modiolus Distance on Electrophysiological and Psychophysical Parameters in CI Patients With Perimodiolar and Lateral Electrode Arrays. *Otology & Neurotology* **41**, e1091-e1097 (2020).
59. Rau, T. S. et al. Histological evaluation of a cochlear implant electrode array with electrically activated shape change for perimodiolar positioning. *Current Directions in Biomedical Engineering* **4**, 145-148 (2018).
60. Battmer, R. D., Zilberman, Y., Haake, P. & Lenarz, T. Simultaneous Analog Stimulation (SAS)--Continuous Interleaved Sampler (CIS) pilot comparison study in Europe. *Ann Otol Rhinol Laryngol Suppl* **177**, 69-73 (1999).
61. Shaul, C. et al. Slim, modiolar cochlear implant electrode: Melbourne experience and comparison with the contour perimodiolar electrode. *Otology & Neurotology* **41**, 639-643 (2020).
62. Todt, I., Basta, D., Eisenschenk, A. & Ernst, A. The "pull-back" technique for Nucleus 24 perimodiolar electrode insertion. *Otolaryngology—Head and Neck Surgery* **132**, 751-754 (2005).
63. Basta, D., Todt, I. & Ernst, A. Audiological outcome of the pull- back technique in cochlear implantees. *The Laryngoscope* **120**, 1391-1396 (2010).